Letter

Cucumber mosaic virus 2b directs fibrillarin translocation to plasmodesmata to promote viral movement

Introduction

Cucumber mosaic virus (CMV) is one of the most widespread and infectious plant viruses affecting over 1200 plant species, including both monocots and dicots (Palukaitis *et al.*, 1992; Mochizuki & Ohki, 2011). The CMV genome consists of three positive-stranded RNAs encoding five proteins: 1a, 2a, 2b, 3a, and coat protein (CP; Jacquemond, 2012). Among them, the multifunctional 2b protein regulates diverse processes throughout the viral life cycle, including viral movement both locally and systemically (Nemes *et al.*, 2014), symptom development (Lewsey *et al.*, 2009), and suppression of RNA silencing as part of the host defense response (Ji & Ding, 2001; Zhang *et al.*, 2006; Zhou *et al.*, 2014).

The 2b proteins of subgroup IA CMV strains, including Fenny Dale (Fny)-CMV strain and Shangdong (SD)-CMV strain, are known to partition between the nucleus and the cytoplasm, yet the biological relevance of such phenomena remains uncertain. Nuclear targeting of 2b proteins from subgroup IA strains is governed by two nuclear localization signals (NLSs), NLS1 and NLS2 (Wang *et al.*, 2004; González *et al.*, 2010; Duan *et al.*, 2012). It was previously shown that NLS mutations impaired 2b's functions in RNA silencing suppression and virus pathogenicity (Lucy *et al.*, 2000; Wang *et al.*, 2004; Lewsey *et al.*, 2009; González *et al.*, 2010). Interestingly, other studies suggested that Fny2b fused with a nuclear export signal, which inhibits its sustained nuclear accumulation, still retains virus silencing suppressor (VSR) activity, suggesting that nuclear localization is not strictly required for this function (González *et al.*, 2012). On the other hand, increasing 2b's nuclear accumulation can reduce its VSR activity while enhancing viral virulence (Du *et al.*, 2014). These findings suggest that the NLS motifs may have broader implications in 2b functionality, potentially beyond its role in VSR activity.

Emerging evidence indicates that the ability of certain viral proteins to form liquid–liquid phase-separated (LLPS) condensates is essential for multiple aspects of the viral lifestyle, including enhancing replication, movement, and host manipulation (Etibor *et al.*, 2021; May, 2024). These condensates act as dynamic compartments, organizing viral and host components to enhance the efficiency of viral gene functions. Liquid–liquid phase-separated-driven interactions between viral proteins and host factors have been shown to facilitate the systemic infection of various plant viruses (Brown *et al.*, 2021). Nevertheless, whether CMV-2b proteins are capable of forming condensates and to what extent such capabilities contribute to its dynamic interactions with host factors and, moreover, to the viral pathogenicity remain largely unknown.

Fibrillarin (FIB), a key plant nucleolar protein involved in RNA processing, has been implicated in regulating the movements of different RNA viruses (Canetta *et al.*, 2008; Hipper *et al.*, 2013; Li *et al.*, 2018; Decle-Carrasco *et al.*, 2021). In *Arabidopsis thaliana* (hereafter Arabidopsis), silencing of *FIB2* impeded the long-distance transport of umbravirus, groundnut rosette virus (GRV) (Souza & Carvalho, 2019). Together with GRV-ORF3 protein, FIB2 associates with viral RNA to form Ribonucleoprotein (RNP) particles, which are then transported from cell to cell, ultimately completing long-distance trafficking (Kim *et al.*, 2007). Similarly, the P26 movement protein from *Pea enation mosaic virus 2* (PEMV2) interacts with FIB2, forming droplets with PEMV2 genomic RNAs *in vitro* for systemic virus movement (Brown *et al.*, 2021). These examples suggest that phase-separated droplets play an important role in virus–host interactions. However, the role of FIB2 protein during CMV infection, particularly in the context of viral protein interactions, remains to be determined.

Here, we show that CMV-2b forms condensates *in planta*, which are driven by its NLS motifs, and these two NLS domains are crucial for interaction of 2b with FIB2 proteins. Additionally, FIB2 proteins positively regulate CMV infection lifecycle and are required for 2b protein-dependent LLPS formation *in vivo*. Our findings reveal that the formation of 2b condensates and the translocation of 2b/FIB2 complex to the plasmodesmata (PD) are essential for facilitating viral cell-to-cell movement and promoting CMV infection.

Materials and Methods

Plant materials and virus inoculation

Nicotiana benthamiana Domin and Arabidopsis *thaliana* (L.) plants, including wild-type and *fib2* mutant (Salk_093373C, ABRC), were grown at 22°C under a 16-h : 8-h, light : dark photoperiod. The virus used was the SD-CMV strain. The 35S-CMV-R1, 35S-CMV-R2, and 35S-CMV-R3 constructs were co-infiltrated into leaves of 3-wk-old Nicotiana plants following the method described by Hou *et al.* (2011). Systemically infected leaves were harvested for virus maintenance.

Crude sap from CMV-infected *N. benthamiana* leaves was prepared by grinding leaves in 0.01 M phosphate buffer (pH 7.0). The 3rd and 4th leaves of 14-d-old Arabidopsis seedlings were dusted with carborundum powder and inoculated with the sap. Mock-inoculated plants were inoculated with buffer only. For each genotype, 40 plants were used per experiment, and all assays were repeated three times.

Plasmid constructs

2b sequence (UniProt sequence ID, P0C783) and its deletion constructs (ΔNLS1, ΔNLS2, ΔNLS1/2) were synthesized (Biobasic Co., Markham, ON, Canada) and cloned into pENTY vectors via Bacteriophage P1 (BP) cloning. Coding sequences of Arabidopsis *FIB1*, *FIB2*, and its truncated forms (FIB2-glycine- and arginine-rich (GAR) [1-77aa] and FIB2-ΔGAR [78-320aa]) were polymerase chain reaction (PCR)-amplified from Arabidopsis cDNA and cloned into pENTY vectors. Control genes barely any meristem 1 (*BAM1)* and plasmodesmata-localized protein 5 (*PDLP5*; Tran & Citovsky, 2021) were also cloned into pENTY using the Gateway system. Recombinant expression vectors were constructed as follows.

For protein expression and *in vitro* interaction assays: *2b*-Δ*NLS1*, -Δ*NLS2*, -Δ*NLS1/2* were introduced into pET-28aSUMO-mCherry vector; *AtFIB2* was cloned into pET-28aSUMO-*mEGFP*; *FIB1*, *FIB2-GAR*, and *AtFIB2*-Δ*GAR* were cloned into MBP-DC vector using Lambda Recombination (LR) cloning (Thermo Fisher Scientific, Waltham, MA, USA).

For subcellular localization analysis: *2b*-Δ*NLS1*, -Δ*NLS2*, and -Δ*NLS1/2* were cloned into pBA-GFP-DC; *FIB2* and *PDLP5* were cloned into pBA-DC-GFP; *BAM1*, 2b, and *At-coilin* were cloned into pBA-DC-CFP.

For bimolecular fluorescence complementation (BiFC) assay: *2b* and its variants were cloned into pBA-GFP^{N}-DC vectors; *FIB2* was cloned into pBA-DC-GFP^{C}.

For yeast two-hybrid (Y2H) experiments: *2b* was cloned into pGBT9-DC as BD-2b; *FIB1* and *FIB2* were cloned into pGAD424-DC.

For RNAi experiments: a 321-bp fragment (regions 501–821) of the *NbFIB2* gene (AM269909) and the β-glucuronidase (*GUS)* coding fragment were cloned into pK7WG2 for silencing in Nicotiana.

Primers used in this study are shown in Supporting Information Table S1. The amino acids of 2b variants are shown in Table S2. All constructs were confirmed by sequencing.

Agrobacterium-mediated transient overexpression (OE)

Binary vectors were transformed into Agrobacterial GV3101. Colonies were grown overnight in liquid LB medium, harvested, and resuspended in the Agrobacterium resuspension buffer (10 mM $MgCl_2$, 10 mM 2-(*N*-morpholino)ethanesulfonic acid (MES), and 0.2 mM acetosyringone) to an OD_{600} of *c.* 1.0. After a 2–3 h incubation, bacterial suspensions were infiltrated into Nicotiana leaves using a 1-ml syringe without a needle. Fluorescence signals were visualized 2 d postinfiltration using a confocal microscope (Olympus FV3000 confocal laser scanning microscope; Evident Corporation, Waltham, MA, USA).

For PD visualization, aniline blue (0.1 mg ml^{-1}; Sigma) was infiltrated into leaves and observed under a confocal microscope using 488 and 406 nm excitation wavelengths for GFP, Cyan Fluorescent Protein (CFP), and aniline blue staining, respectively.

Protein expression and purification

Expression constructs were transformed into *Escherichia coli* strain Rosetta (Novagen/Merck, Darmstadt, Germany) and proteins were purified according to previous reports (Park *et al.*, 2019) with modifications. Briefly, induced cells were suspended in lysis buffer (50 mM Tris–HCl pH 7.4, 200 mM NaCl, 1 mM $MgCl_2$, 1 mg ml^{-1} lysozyme, 10% Glycerol) and gently shaken for 30 min in a cold room. Bacterial cells were broken by sonication (Qsonica, Newtown, CT, USA) on ice at 40% amplitude, 15 s on/30 s off, 15 cycles, and TritonX100 was then added to a final concentration of 1%. Cell lysates were centrifuged at 21 000 ***g*** for 1 h (Beckman Coulter, Pasadena, CA, USA). The supernatant was mixed with equilibrated amylose (NEB, Ipswich, MA, USA) or Ni-NTA beads (Bio Basic Inc., Markham, ON, Canada), and manufacturers' instructions were followed to obtain purified proteins.

His-SUMO fluorescence-tagged proteins were cleaved with the ULP1 enzyme and further purified to homogeneity with reverse Heparin chromatography (Cytiva, Marlborough, MA, USA). Protein purity was assessed by SDS-PAGE.

In vitro phase separation assays

Droplet formation assays were performed with indicated concentrations of recombinant protein, 10 mM Tris–HCl (pH 7.5), 1 mM dithiothreitol (DTT), and 100 mM NaCl, with or without 10% PEG-4000. Samples were directly observed using an Olympus FV3000 confocal microscope (40× objective, 543 nm excitation).

For the salt-resistance assay, 5 M NaCl was added to the induced liquid droplets to achieve a final concentration of 1 M, and the effect on droplet stability was observed.

1,6-Hexanediol (HEX) at a purity of 99% was purchased from Sigma-Aldrich (#240117), heated to 45°C, adjusted to a 50% stock solution in water, and mixed at room temperature (RT) in 20% (v/v) with protein samples.

In vitro pull-down assay

Five hundred nanograms of purified proteins were incubated in reaction buffer (20 mM Tris–HCl pH 7.4, 150 mM NaCl, 0.2% glycerol, and protease inhibitor (Roche)) for 1 h at RT. Equilibrated resins were then added to the mix, which was further incubated for 1 h at RT. Resins with bound proteins were washed five times with the reaction buffer. Bound proteins were eluted by NuPAGE buffer (Thermo Fisher Scientific) containing lithium dodecyl sulfate at pH 8.5 and incubated at 98°C for 5 min. Samples were analyzed by SDS-PAGE followed by Western blot analysis using α-MBP and α-2b (ABClonal Co., Wuhan, Hubei, China).

Yeast two-hybrid assay

Constructs were transformed into *Saccharomyces cerevisiae* strain AH109 according to the manufacturer's instructions (Clontech,

New Phytologist

Moutain View, CA, USA). Transformed cells were spotted on Sabouraud's dextrose (SD)/-Ade/-His/-Leu/-Trp quadruple deficient medium to examine for protein–protein interaction.

RNA expression analysis

Total RNAs of *GUS-RNAi* and *NbFIB-RNAi* lines were extracted using RNA mini kits (Qiagen N.V., Hilden, Germany). Reverse transcription (RT) was performed with 1 μg RNA using the iScript cDNA synthesis kit (Bio-Rad Laboratories, Inc., Hercules, CA, USA) following the manufacturer's instructions. The cDNA solution was diluted (1 : 2) with nuclease-free water. Quantitative PCR was performed using SYBR Green Master (Bio-Rad) on the Bio-Rad CFX96 real-time system for 40 cycles using quantitative PCR primers for *Nb-actin*, *NbFIB2*, and *CMV-CP*. Primer pairs used are listed in Table S1.

Generation of transgenic plants

To generate AtFIB2 overexpression (OE) plant, the AtFIB2 coding sequence was cloned into pBA-DC-GFP vector, which was transcribed by a CaMV 35S promoter (Odell *et al.*, 1985) in the WT (Col-0) background.

FIB-RNAi and *GUS-RNAi* transgenic *Nicotiana* plants were generated by transformation with *Agrobacterium tumefaciens* carrying the plasmid. Procedures for the transformation and regeneration of transgenic *Nicotiana* plants were performed according to the previous report (Topping, 1998). Transgenic plants were selected on 200 mg l^{-1} kanamycin. At least three independent RNAi lines were selected for each construct.

Cell-to-cell movement assays of CMV 2b

2b-GFP vector was transformed into GV3101 strain and infiltrated into *Nicotiana* with OD_{600} of Agrobacterium cell suspension ranging from 10^{-5} to 10^{-4}. These conditions were optimized for expression in single transformed cells. Two or three days later, the infiltrated leaves were harvested and observed using a laser scanning confocal microscope with ×10 and ×40 objective lenses and Green Fluorescence Protein (GFP) filter. Single cells (indicating no cell-to-cell movement) and clusters of two and three cells containing the GFP signal (indicating cell-to-cell movement) were scored in at least three different leaves from three different plants.

Statistics and reproducibility

All representative images reflect a minimum of three biological replicates. The quantitative data in Figures were derived from at least three independent biological experiments. The exact number of biological replicates performed per experiment are indicated in the figure legends. Statistical significance of differences in sample means was evaluated by two-tailed *t*-test using Excel 2019 (Microsoft Corporation, Redmond, WA, USA) software. *P*-values of < 0.01 with the statistical probability of $> 99\%$ were considered statistically significant.

Results and Discussion

Intrinsically disordered regions and NLSs drive CMV-2b phase separation

Given the pivotal role of intrinsically disordered regions (IDRs) in driving LLPS formation, to investigate whether phase separation of the CMV-2b protein is similarly regulated by IDRs, we screened the CMV 2b sequence with multiple IDR prediction programs, IUPred and PrDOS (Ishida & Kinoshita, 2007; Dosztányi, 2018). Our analysis uncovered an arginine-rich disordered region spanning amino acids 20–40 of the CMV-2b protein, which encompasses both NLS1 and NLS2 (Fig. S1a,b), suggesting that these regions may play a critical role in promoting 2b-mediated LLPS.

To this end, we generated recombinant mCherry-tagged 2b proteins, including wild-type (2b-WT) and NLS-deleted variants (ΔNLS1, ΔNLS2, and ΔNLS1/2). Their size and purity were confirmed with gel electrophoresis (Fig. S1c). *In vitro* phase separation assays demonstrated that 2b-WT readily formed condensates, in contrast to mCherry alone, which exhibited a diffusion pattern (Fig. 1a). Deletion of either NLS1 or NLS2 partially disrupted droplet formation, which could be restored upon the addition of 10% PEG4000, a crowding agent. Notably, the ΔNLS1/2 mutant exhibited a diffuse pattern, even in the presence of PEG4000, highlighting the essential role of both NLS1 and NLS2 in driving LLPS under physiological conditions.

To further explore the biophysical properties of 2b-WT droplets, we examined their sensitivity to changes in ionic strength and hydrophobic interactions. The condensates dissolved in the presence of 1 M NaCl, indicating that electrostatic interactions are critical for droplet stability. Additionally, treatment with 20% HEX, a reagent known to disrupt hydrophobic interactions, effectively inhibited droplet formation (Fig. 1b).

Together, these findings demonstrate that the NLS regions are integral to 2b protein condensate formation. While the single NLS deletions require a crowded environment to drive phase separation, complete deletion of both NLS abolishes condensate formation entirely. The sensitivity of 2b-WT droplets to salt and HEX further underscore the importance of electrostatic and hydrophobic interactions in maintaining 2b LLPS *in vitro*.

To explore the roles of the 2b NLS regions in promoting LLPS *in planta*, we transiently expressed GFP-fused 2b variants (2b-WT and NLS mutants ΔNLS1, ΔNLS2, and ΔNLS1/2) in *N. benthamiana* (hereafter Nicotiana) under the control of a Cauliflower mosaic virus 35S promoter. Consistent with previous reports, 2b-WT localized to both the cytoplasm and the nucleus, and similar patterns were observed for ΔNLS1 and ΔNLS2 proteins (Fig. 1c). By contrast, ΔNLS1/2 was exclusively cytoplasmic (Fig. 1c). Importantly, nuclear condensates formed only in plants expressing 2b-WT, whereas neither ΔNLS1 nor ΔNLS2 mutants showed nuclear droplet formation, aligning with *in vitro* results (Fig. 1a,c). Furthermore, these nuclear condensates were distinct from Cajal bodies, as they did not co-localize with Coilin-CFP (Fig. S1d). These findings collectively indicate critical roles of NLS1 and NLS2 in both mediating 2b phase separation and functional subcellular localization *in planta*.

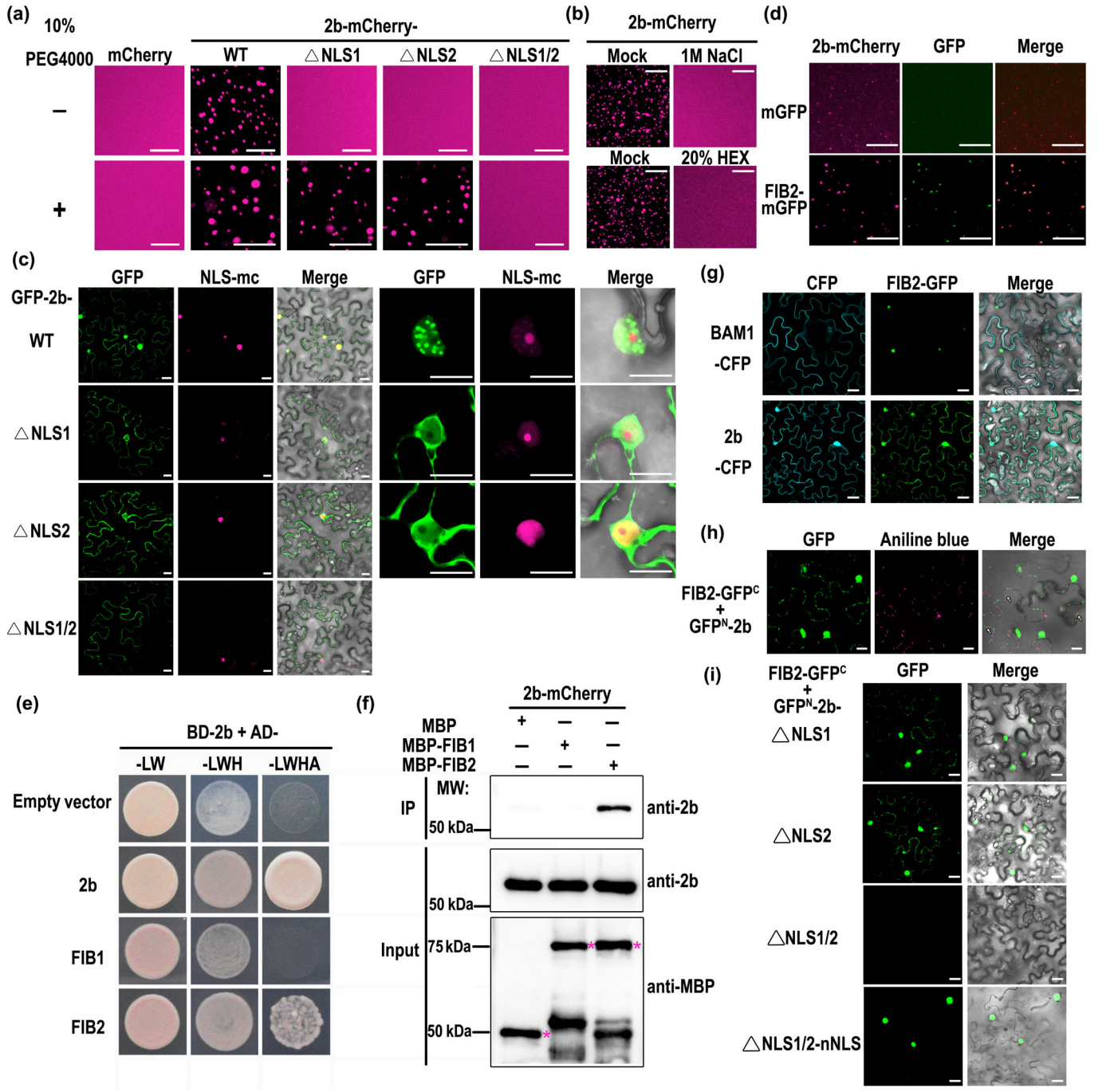

Fig. 1 Cucumber mosaic virus (CMV)-2b undergoes liquid–liquid phase separated (LLPS) via its nuclear localization signals (NLSs) and interacts with AtFIB2. (a, b) *In vitro* droplet formation visualized by confocal microscopy. (a) LLPS of 8 μM monomeric Cherry (mCherry)-tagged 2b-wild-type (WT), and nuclear localization signal (NLS) variants were assessed in the presence or absence of 10% PEG4000 as a crowding agent. mCherry alone served as a negative control. Bars, 10 μm. (b) Treatment of 2b-WT-mCherry with 1 M NaCl or 20% hexanol. Bars, 20 μm. (c) Subcellular localization of CMV-2b and its NLS variants. Nicotiana leaves were co-infiltrated with Agrobacterium strains carrying *35S-GFP-2b-WT* or *35S-GFP-2b-NLS* variants and *35S-NLS-mc* (mCherry tagged with an NLS) as a nuclear marker. Bars, 20 μm. (d) *In vitro* co-localization of mGFP-fibrillarin 2 (FIB2) (1 μM) and 2b-mCherry (1 μM) mixture. Bars, 10 μm. (e) Yeast two-hybrid assays testing interaction between 2b and FIB1 or FIB2. Interaction clones were selected on the synthetic dropout medium (SD/-Leu/-Trp/-His and SD/-Leu/-Trp/-His/-Ade). (f) Pull-down assay showing *in vitro* interaction between 2b and FIB1 or FIB2. Recombinant 2b-mCherry protein was incubated with Maltose Binding Protein (MBP), MBP-FIB1, or MBP-FIB2 bound to MBP agarose beads, followed by detection using anti-2b antibody. A red asterisk indicates the target protein band. (g) Subcellular localization of FIB2-GFP in the presence of *35S-BAM1-CFP* or *35S-2b-CFP* in *Nicotiana benthamiana* leaves. Bars, 10 μm. (h) bimolecular fluorescence complementation (BiFC) assay showing the interaction between FIB2-GFP^C and GFP^N-2b in *N. benthamiana* leaves. Aniline blue was used as a plasmodesmata (PD) marker. Arrowheads indicate the co-localized punctate pattern in PD. Bars, 20 μm. (i) BiFC assay to test possible interactions between FIB2-GFP^C and GFP^N-2b-NLS variants (-ΔNLS1, -ΔNLS2, or -ΔNLS1/2). Fluorescence signals were imaged 2 d postinfiltration in *N. benthamiana* leaves. Bars, 20 μm. HEX, 1,6-hexanediol. GFP, green fluorescence protein; CFP, cyan fluorescence protein.

New Phytologist

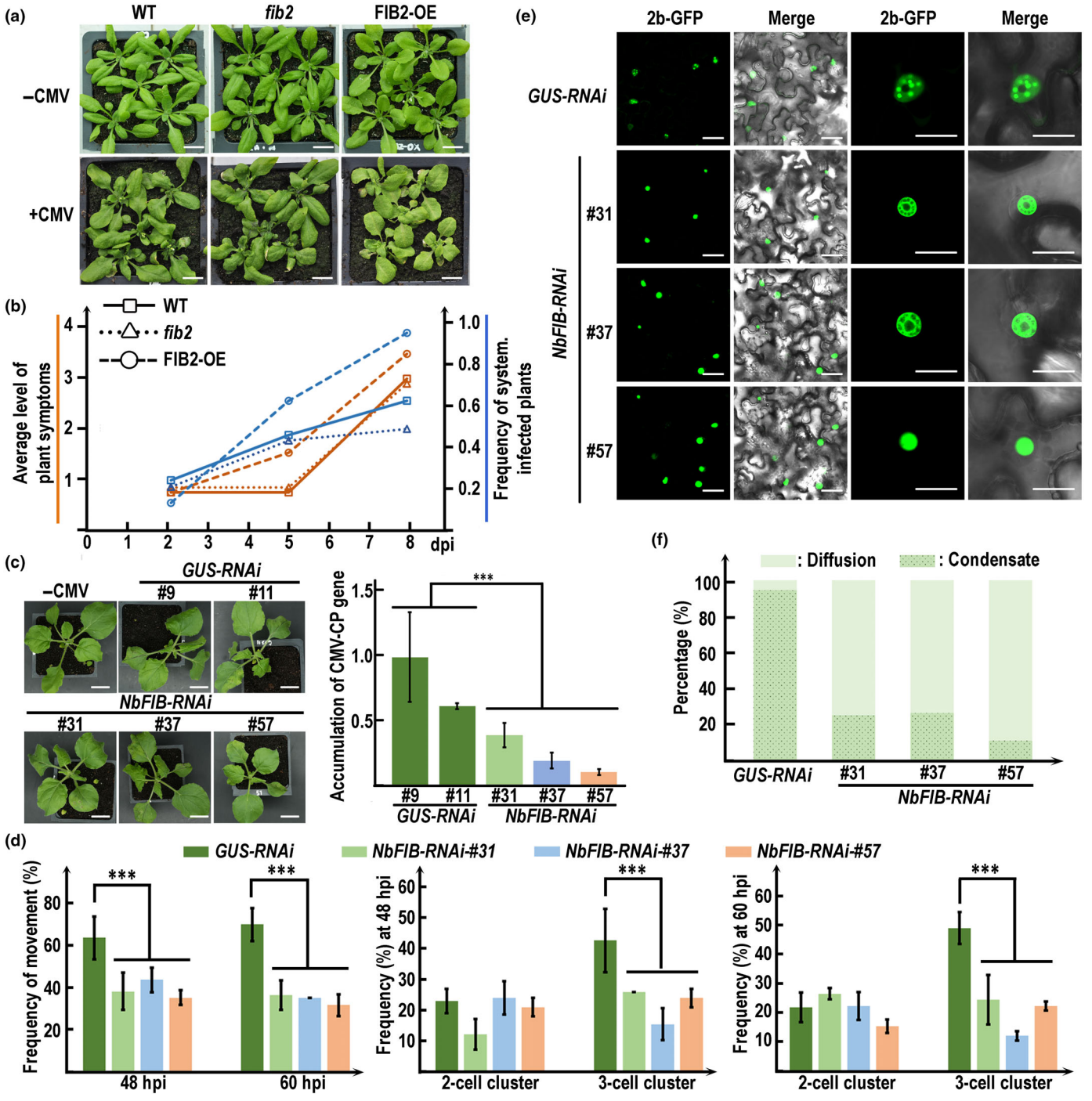

FIB forms phase-separated condensates and interacts with CMV-2b

Fibrillarin 2 is a nucleolar protein with an intrinsically disordered GAR domain that can form droplets *in vitro* (Rakitina *et al.*, 2011; Guillen-Chable *et al.*, 2020; Brown *et al.*, 2021). In line with previous reports, we observed that GFP-tagged Arabidopsis FIB2 proteins readily formed condensates under crowding conditions (10% PEG4000, Fig. S1e). To determine possible interactions between CMV-2b and FIB2, 2b-mCherry was added to pre-formed FIB2-mGFP droplets at a 1 : 1 molar ratio. Fig. 1d shows that the two proteins co-localized within the condensates, demonstrating that 2b-mCherry partitioned into FIB2-mGFP droplets via a potential interaction between these two proteins.

Using Y2H and *in vitro* pull-down assays, we confirmed that 2b directly interacted with FIB2, but not FIB1, the other fibrillarin isoform in Arabidopsis (Rakitina *et al.*, 2011; Zheng *et al.*, 2018; Seo *et al.*, 2019; Decle-Carrasco *et al.*, 2021) (Fig. 1e,f). Pull-down

Fig. 2 Silencing of fibrillarin (FIB) suppresses cucumber mosaic virus (CMV) movement. (a) Phenotypes of CMV-infected Arabidopsis wild-type (WT), *fib2* mutant, and FIB2 overexpression (FIB2-OE) seedlings. Photographs were taken at 10 dpi, days postinfection (dpi). The areas of typical yellowish and curled young leaves represent the degree of disease symptoms. Bar, 1 cm. (b) Infectivity (blue, frequency of systemically infected plants) and disease progression (orange) curves. The increase in incidence and progression of symptom severity for WT, *fib2* mutant, and FIB2-OE lines were compared (Butković *et al*., 2021; Martínez *et al*., 2023). (c) CMV symptoms (left panel) and coat protein (CP) expression (right panel) in *GUS-RNAi* and *NbFIB-RNAi* transgenic *Nicotiana benthamiana* lines. Bar, 3 cm. CMV–CP expression levels were quantified by quantitative reverse transcription polymerase chain reaction, normalized to *Nb-actin*. Error bars represent ± SD. Statistically significant differences between *NbFIB-RNAi* and *GUS-RNAi* plants are indicated (two-tailed *t*-test: ***, $P < 0.01$). (d) Cell-to-cell movement of CMV 2b in *NbFIB-RNAi* plants. Constructs expressing 2b-GFP or PDLP5-GFP (cell-autonomous control; Tran & Citovsky, 2021) were agroinfiltrated into *GUS-RNAi* and *NbFIB-RNAi* leaf tissues. Images were recorded 48 h postagroinfiltration (hpi) and were single confocal sections representative of multiple independent experiments ($n = 20$ images from five plants). Cell-to-cell movement frequency (left panel) was quantified by scoring GFP signal-containing cell clusters at 48 and 60 hpi in both *GUS-RNAi* and *NbFIB-RNAi* plants. The extent of 2b-GFP movement at 48 hpi (middle panel) and 60 hpi (right panel) was scored as the frequency of cell clusters containing 2–3 GFP-positive cells/cluster. Error bars represent ±SD from three biological replicates. Asterisks indicate statistically significant differences between the *NbFIB-RNA*i plants and the control *GUS-RNAi* plants. Two-tailed *t*-test: ***, $P < 0.01$. (e) Nuclear-localized pattern of 2b-GFP in *NbFIB-RNAi* and the *GUS-RNAi* plants. 2b-GFP was transiently expressed in leaves of *NbFIB-RNAi* and *GUS-RNAi*. GFP signal pattern in the nucleus was observed at 48 hpi by confocal scanning laser microscopy. Bar, 20 μm (left panel, 10× magnification; right panel, 60× magnification). Images are single confocal sections representative of multiple independent experiments ($n = 30$ images from five plants). (f) Quantification of the percent of 2b-GFP in condensate vs diffused status in *NbFIB-RNAi* and *GUS-RNAi* plants (as shown in e). Data are representative of multiple independent experiments ($n = 30$ images from five individual lines). GUS, β-glucuronidase; GFP, green fluorescence protein.

assays with truncated FIB2 constructs further suggested that 2b bound to the C-terminal ΔGAR domain but not the N-terminal GAR (Fig. S2a). To further verify the interactions between 2b and FIB2 *in planta*, colocalization and BiFC assays were performed.

Intriguingly, while FIB2-GFP localized in the nucleus, 2b and FIB2 were co-localized in both the nucleus and cytosol, indicating that 2b facilitated FIB2 nuclear export (Fig. 1g). *In vivo* aniline blue staining assays further suggested that cytosolic 2b/FIB2 complexes were associated with PD (Fig. 1h). Collectively, these results indicate that the CMV-2b protein directly associates with nuclear FIB2 and mediates its nuclear export to PD.

NLS regions mediate 2b-AtFIB2 interaction and nuclear export

Given that the NLSs of CMV-2b are essential for its *in planta* functions and LLPS properties, we next investigated the role of NLSs in CMV-2b–FIB2 interaction and FIB2 nuclear export. Consistent with their nuclear localizations, both the ΔNLS1 and ΔNLS2 mutants maintained their ability to interact with FIB2. By contrast, the ΔNLS1/2 double mutant neither localized to the nucleus nor interacted with FIB2, as demonstrated by *in planta* BiFC and *in vitro* pull-down assays, respectively (Figs 1c,i, S2b). Remarkably, restoring the nuclear localization of the ΔNLS1/2-*n*NLS (ΔNLS1/2 mutant by adding a synthetic NLS peptide (LGKRKW)) failed to restore this interaction in the cytoplasm (Fig. 1i). Together, these results underscore the critical role of the NLS motifs of 2b in facilitating not only the nuclear localization but also the nuclear exit of the 2b/FIB2 complex to the cytosol (Fig. 1i).

FIB2 translocation and its role in CMV infection

The CMV-2b-mediated re-localization of FIB2 to cytoplasmic inclusions suggests that FIB2 is likely involved in the CMV infection process. To test the biological relevance of FIB2 in plant–virus interaction, Nicotiana leaves preinfiltrated with FIB2-GFP were infected with a CMV strain. FIB2-GFP localized exclusively to the nucleus at 0 h postinfection (hpi), consistent with its nucleolar role. Notably, by 58 hpi, the FIB2-GFP signal was observed in the cytosol of CMV-infected leaves, a pattern not found in the mock-treated control (Fig. S2c). The cytosolic localization persisted at 72 hpi, indicative of the involvement of FIB2 during CMV infection. To explore the role of CMV-2b in FIB2 translocation, we infected Nicotiana leaves with CMVΔ2b strain, which carries a 2b deletion. Intriguingly, unlike the WT strain, CMVΔ2b strain, which does not contain the 2b gene, failed to induce the nucleus-to-cytosol partitioning of FIB2-GFP (Fig. S2c). These results demonstrate that 2b mediates FIB2 nuclear export, suggesting a functional interaction between FIB2 and CMV-2b during CMV infection.

FIB2 enhances CMV infection in Arabidopsis and Nicotiana

We further assessed the functional relevance of FIB2 in CMV infection in Arabidopsis. WT Arabidopsis plants, *fib2* knockout mutants, and FIB2-OE plants were infected with CMV, and the infection progression was tracked by measuring systemic infection and symptom severity at 2, 5, and 8 d postinoculation (Fig. 2a,b). Compared to the WT plants, *FIB2*-OE plants exhibited stunted growth, paler green leaves, higher infectivity, and more severe symptom progression upon CMV infection. Conversely, *fib2* mutant plants displayed reduced systemic infection at 5 d postinoculation, suggesting that FIB2 positively regulates CMV infection severity.

To further corroborate these observations and ensure the observed phenotypes were not due to mechanical injury during CMV infection by leaf rubbing, we performed CMV infection assays in Nicotiana *NbFIB-RNAi* knockdown plants. Consistent with the previously observed results in Arabidopsis, *NbFIB-RNAi* knockdown plants exhibited milder symptoms and reduced CMV-CP mRNA accumulation compared to the *GUS-RNAi* control (Figs 2c, S3a). These findings highlight the conserved role of FIB2 proteins in promoting CMV infection across Solanaceae and Brassicaceae.

FIB2 is essential for CMV-2b movement and phase separation *in vivo*

To further understand the involvement of FIB2 during CMV infection in a 2b-dependent fashion, we examined the cell-to-cell transport of GFP-tagged 2b in tobacco plants expressing *GUS-RNAi* and *NbFIB-RNAi*. 2b-GFP was observed to move from cell to cell; by contrast, the expression of a GFP-tagged Arabidopsis PDLP5 protein, known to be associated with PD but not to move between cells (Thomas *et al.*, 2008; Lee *et al.*, 2011; Wang *et al.*, 2013; Liu *et al.*, 2020), produced only single cells with a GFP signal (Fig. S3b). To quantify the capability of cell-to-cell movement, 2b-GFP transport was scored based on the appearance of two-cell or three-cell clusters expressing the GFP signal, with the initially expressing cells exhibiting a higher signal intensity than their neighboring cells. We observed CMV 2b-GFP-containing clusters in *c.* 60% of the expressing cells in the control GUS-RNAi plants (Fig. 2d). Notably, the extent of CMV 2b-GFP cell-to-cell movement in *NbFIB-RNAi* plants was significantly reduced, with the formation of three-cell clusters being reduced to 25% in *NbFIB-RNAi* plants, although the signals remained detectable at 60 dpi (Fig. 2d).

Moreover, an altered localization pattern of 2b-GFP was also observed in *NbFIB-RNAi* plants. The ratio of condensate to diffused pattern of 2b-GFP was counted in the nuclei of GUS-RNAi or *NbFIB-RNAi* from at least 8 different infiltrated leaves of each line. We found that 98% of 2b-GFP signals formed condensates in GUS-RNAi plants, which was reduced to < 30% in *NbFIB-RNAi* plants, with most signals appearing diffusely distributed (Fig. 2e,f). These findings indicate that FIB2 facilitates the phase separation of CMV-2b in the nuclei and supports its efficient cell-to-cell movement *in vivo*.

Conclusions

Our data revealed that the CMV-2b protein directly interacts with plant fibrillarin and forms biomolecular condensates in nuclei in an NLS-dependent manner. Notably, these condensates do not contain coilin and therefore are distinct from the Cajal bodies. CMV-2b facilitates the nuclear export of FIB2 during CMV infection, and this nuclear-cytoplasmic re-localization of FIB2 is critical for the infection process. Genetic evidence from both Arabidopsis and Nicotiana further demonstrates that CMV leverages host FIB2 proteins to promote the efficient spread of the virus.

From a mechanism perspective, we show that FIB2 enhances the cell-to-cell movement of CMV-2b and facilitates its LLPS *in vivo*. The disruption of FIB2 function significantly reduces 2b condensate formation in nuclei and impairs its intercellular movement. These findings suggest that phase separation of 2b, supported by FIB2, is essential for the systemic spread of CMV. Furthermore, the reduced infectivity and mild symptoms associated with the CMV-2bΔNLS1/2 mutant strain, as previously reported (Lewsey *et al.*, 2009), can now be attributed not only to the loss of its silencing suppressor activity but also to the impaired cell-to-cell movement caused by its disrupted condensate formation.

Collectively, our work identified plant FIB2 proteins as essential host factors that facilitate CMV infection and uncovered the molecular mechanism underlying the CMV-2b-FIB2 interaction. By demonstrating the role of phase separation in viral movement, this study provides new insights into the interplay between host nucleolar proteins and plant viruses, advancing our understanding of viral pathogenesis and host–virus interactions.

Acknowledgements

We thank Prof. Huishan Guo (State Key Laboratory of Plant Genomics, China) for providing the SD-CMV strain. We are also grateful to our former colleague Steven Lehung Cheng for his guidance on LLPS and Chunghao Huang for his assistance with virus-related instructions. This work was supported by the core funding from Temasek Life Sciences Laboratory and Disruptive and Sustainable Technology for Agriculture Precision (DiSTAP), an interdisciplinary research group of the Singapore MIT Alliance for Research and Technology (SMART) Center supported by the National Research Foundation (NRF), Prime Minister's Office, Singapore, under its Campus for Research Excellence and Technological Enterprise (CREATE) program.

Competing interests

None declared.

Author contributions

DZ and NHC designed the experiments. DZ and HYX executed the experiments. DZ and NHC wrote the manuscript.

ORCID

Nam-Hai Chua https://orcid.org/0000-0002-8991-0355
Dan Zhang https://orcid.org/0009-0002-1658-5675

Data availability

Data sharing is not applicable to this article as no new data were created or analyzed in this study. The 2b protein sequence used in this study was obtained from UniProt under sequence ID P0C783. The *N. benthamiana FIB2* mRNA sequence was obtained from GenBank (NCBI, National Center of Biotechnology Information) under sequence ID AM269909.

Dan Zhang, Haiying Xu and Nam-Hai Chua*

Temasek Life Sciences Laboratory, 1 Research Link, National University of Singapore, Singapore, 117604, Singapore
(*Author for correspondence: email chua@rockefeller.edu)

References

Brown SL, Garrison DJ, May JP. 2021. Phase separation of a plant virus movement protein and cellular factors support virus-host interactions. *PLoS Pathogens* **17**: e1009622.

Butković A, Gonzalez R, Rivarez MPS, Elena SF. 2021. A genome-wide association study identifies *Arabidopsis thaliana* genes that contribute to

differences in the outcome of infection with two Turnip mosaic potyvirus strains that differ in their evolutionary history and degree of host specialization. *Virus Evolution* **7**: veab063.

Canetta E, Kim SH, Kalinina NO, Shaw J, Adya AK, Gillespie T, Brown JW, Taliansky M. 2008. A plant virus movement protein forms ringlike complexes with the major nucleolar protein, fibrillarin, *in vitro*. *Journal of Molecular Biology* **376**: 932–937.

Decle-Carrasco S, Rodríguez-Zapata LC, Castano E. 2021. Plant viral proteins and fibrillarin: the link to complete the infective cycle. *Molecular Biology Reports* **48**: 4677–4686.

Dosztányi Z. 2018. Prediction of protein disorder based on IUPred. *Protein Science* **27**: 331–340.

Du Z, Chen A, Chen W, Liao Q, Zhang H, Bao Y, Roossinck MJ, Carr JP. 2014. Nuclear-cytoplasmic partitioning of cucumber mosaic virus protein 2b determines the balance between its roles as a virulence determinant and an RNA-silencing suppressor. *Journal of Virology* **88**: 5228–5241.

Duan CG, Fang YY, Zhou BJ, Zhao JH, Hou WN, Zhu H, Ding SW, Guo HS. 2012. Suppression of *Arabidopsis* ARGONAUTE1-mediated slicing, transgene-induced RNA silencing, and DNA methylation by distinct domains of the cucumber mosaic virus 2b protein. *Plant Cell* **24**: 259–274.

Etibor TA, Yamauchi Y, Amorim MJ. 2021. Liquid biomolecular condensates and viral lifecycles: review and perspectives. *Viruses* **13**: 366.

González I, Martínez L, Rakitina DV, Lewsey MG, Atencio FA, Llave C, Kalinina NO, Carr JP, Palukaitis P, Canto T. 2010. Cucumber mosaic virus 2b protein subcellular targets and interactions: their significance to RNA silencing suppressor activity. *Molecular Plant–Microbe Interactions* **23**: 294–303.

González I, Rakitina D, Semashko M, Taliansky M, Praveen S, Palukaitis P, Carr JP, Kalinina N, Canto T. 2012. RNA binding is more critical to the suppression of silencing function of cucumber mosaic virus 2b protein than nuclear localization. *RNA* **18**: 771–782.

Guillen-Chable F, Corona UR, Pereira-Santana A, Bayona A, Rodríguez-Zapata LC, Aquino C, Šebestová L, Vitale N, Hozak P, Castano E. 2020. Fibrillarin ribonuclease activity is dependent on the GAR domain and modulated by phospholipids. *Cells* **9**: 1143.

Hipper C, Brault V, Ziegler-Graff V, Revers F. 2013. Viral and cellular factors involved in phloem transport of plant viruses. *Frontiers in Plant Science* **4**: 154.

Hou WN, Duan CG, Fang RX, Zhou XY, Guo HS. 2011. Satellite RNA reduces expression of the 2b suppressor protein resulting in the attenuation of symptoms caused by cucumber mosaic virus infection. *Molecular Plant Pathology* **12**: 595–605.

Ishida T, Kinoshita K. 2007. PrDOS: prediction of disordered protein regions from amino acid sequence. *Nucleic Acids Research* **35**: W460–W464.

Jacquemond M. 2012. Cucumber mosaic virus. *Advances in Virus Research* **84**: 439–504.

Ji LH, Ding SW. 2001. The suppressor of transgene RNA silencing encoded by cucumber mosaic virus interferes with salicylic acid-mediated virus resistance. *Molecular Plant–Microbe Interactions* **14**: 715–724.

Kim SH, Macfarlane S, Kalinina NO, Rakitina DV, Ryabov EV, Gillespie T, Haupt S, Brown JW, Taliansky M. 2007. Interaction of a plant virus-encoded protein with the major nucleolar protein fibrillarin is required for systemic virus infection. *Proceedings of the National Academy of Sciences, USA* **104**: 11115–11120.

Lee JY, Wang X, Cui W, Sager R, Modla S, Czymmek K, Zybaliov B, van Wijk K, Zhang C, Lu H *et al.* 2011. A plasmodesmata-localized protein mediates crosstalk between cell-to-cell communication and innate immunity in Arabidopsis. *Plant Cell* **23**: 3353–3373.

Lewsey M, Surette M, Robertson FC, Ziebell H, Choi SH, Ryu KH, Canto T, Palukaitis P, Payne T, Walsh JA *et al.* 2009. The role of the cucumber mosaic virus 2b protein in viral movement and symptom induction. *Molecular Plant–Microbe Interactions* **22**: 642–654.

Li Z, Zhang Y, Jiang Z, Jin X, Zhang K, Wang X, Han C, Yu J, Li D. 2018. Hijacking of the nucleolar protein fibrillarin by TGB1 is required for cell-to-cell movement of barley stripe mosaic virus. *Molecular Plant Pathology* **19**: 1222–1237.

Liu NJ, Zhang T, Liu ZH, Chen X, Guo HS, Ju BH, Zhang YY, Li GZ, Zhou QH, Qin YM *et al.* 2020. Phytosphinganine affects plasmodesmata permeability via facilitating PDLP5-stimulated callose accumulation in *Arabidopsis*. *Molecular Plant* **13**: 128–143.

Lucy AP, Guo HS, Li WX, Ding SW. 2000. Suppression of post-transcriptional gene silencing by a plant viral protein localized in the nucleus. *EMBO Journal* **19**: 1672–1680.

Martínez F, Carrasco JL, Toft C, Hillung J, Giménez-Santamarina S, Yenush L, Rodrigo G, Elena SF. 2023. A binary interaction map between turnip mosaic virus and *Arabidopsis thaliana* proteomes. *Communications Biology* **6**: 28.

May JP. 2024. Plant viruses and biomolecular condensates: novel perspectives in virus replication strategies. *New Phytologist* **243**: 1636–1638.

Mochizuki T, Ohki ST. 2011. Cucumber mosaic virus: viral genes as virulence determinants. *Molecular Plant Pathology* **13**: 217–225.

Nemes K, Gellert A, Balazs E, Salanki K. 2014. Alanine scanning of cucumber mosaic virus (CMV) 2b protein identifies different positions for cell-to-cell movement and gene silencing suppressor activity. *PLoS ONE* **9**: e112095.

Odell JT, Nagy F, Chua NH. 1985. Identification of DNA sequences required for activity of the cauliflower mosaic virus 35S promoter. *Nature* **313**: 810–812.

Palukaitis P, Roossinck MJ, Dietzgen RG, Francki RI. 1992. Cucumber mosaic virus. *Advances in Virus Research* **41**: 281–348.

Park SH, Jeong JS, Seo JS, Park BS, Chua NH. 2019. *Arabidopsis* ubiquitin-specific proteases UBP12 and UBP13 shape ORE1 levels during leaf senescence induced by nitrogen deficiency. *New Phytologist* **223**: 1447–1460.

Rakitina DV, Taliansky M, Brown JWS, Kalinina NO. 2011. Two RNA-binding sites in plant fibrillarin provide interactions with various RNA substrates. *Nucleic Acids Research* **39**: 8869–8880.

Seo JS, Diloknawarit P, Park BS, Chua NH. 2019. ELF18-INDUCED LONG NONCODING RNA 1 evicts fibrillarin from mediator subunit to enhance PATHOGENESIS-RELATED GENE 1 (PR1) expression. *New Phytologist* **221**: 2067–2079.

Souza PFN, Carvalho FEL. 2019. Killing two birds with one stone: how do plant viruses break down plant defenses and manipulate cellular processes to replicate themselves? *Journal Of Plant Biology* **62**: 170–180.

Thomas CL, Bayer EM, Ritzenthaler C, Fernandez-Calvino L, Maule AJ. 2008. Specific targeting of a plasmodesmal protein affecting cell-to-cell communication. *PLoS Biology* **6**: e7.

Topping JF. 1998. Tobacco transformation. In: Foster GD, Taylor SC, eds. *Plant virology protocols. Methods in molecular biology™*. Totowa, NJ, USA: Humana Press, 365–372.

Tran PT, Citovsky V. 2021. Receptor-like kinase BAM1 facilitates early movement of the tobacco mosaic virus. *Communications Biology* **4**: 511.

Wang X, Sager R, Cui W, Zhang C, Lu H, Lee JY. 2013. Salicylic acid regulates plasmodesmata closure during innate immune responses in *Arabidopsis*. *Plant Cell* **25**: 2315–2329.

Wang Y, Tzfira T, Gaba V, Citovsky V, Palukaitis P, Gal-On A. 2004. Functional analysis of the cucumber mosaic virus 2b protein: pathogenicity and nuclear localization. *Journal of General Virology* **85**: 3135–3147.

Zhang X, Yuan YR, Pei Y, Lin SS, Tuschl T, Patel DJ, Chua NH. 2006. Cucumber mosaic virus-encoded 2b suppressor inhibits *Arabidopsis* Argonaute1 cleavage activity to counter plant defense. *Genes & Development* **20**: 3255–3268.

Zheng L, He J, Ding Z, Zhang C, Meng R. 2018. Identification of functional domain(s) of fibrillarin interacted with p2 of rice stripe virus. *Canadian Journal of Infectious Diseases and Medical Microbiology* **2018**: 8402839.

Zhou T, Murphy AM, Lewsey MG, Westwood JH, Zhang HM, González I, Canto T, Carr JP. 2014. Domains of the cucumber mosaic virus 2b silencing suppressor protein affecting inhibition of salicylic acid-induced resistance and priming of salicylic acid accumulation during infection. *Journal of General Virology* **95**: 1408–1413.

Supporting Information

Additional Supporting Information may be found online in the Supporting Information section at the end of the article.

Fig. S1 CMV 2b is intrinsically disordered.

Fig. S2 2b interacts with FIB2ΔGAR *in vitro*, and CMV influences FIB2-GFP localization in Nicotiana leaves.

Fig. S3 *NbFIB* expression and localization of 2b-GFP in Nicotiana leaves.

Table S1 Primers used in this study.

Table S2 The protein sequences of 2b-NLS variants in this study.

Please note: Wiley is not responsible for the content or functionality of any Supporting Information supplied by the authors. Any queries (other than missing material) should be directed to the *New Phytologist* Central Office.

Key words: biomolecular condensate, cell-to-cell movement, cucumber mosaic virus, fibrillarin, liquid–liquid phase separation.

Received, 6 January 2025; accepted, 3 February 2025.